[18F]-Fluorodeoxyglucose Positron Emission Tomography/Computed Tomography of LAPC4-CR Castration-Resistant Prostate Cancer Xenograft Model in Soft Tissue Compartments1

Translational Oncology
www.transonc.com

Volume 8 Number 3 June 2015 pp. 147–153 147

[18F]-Fluorodeoxyglucose Positron Emission Tomography/Computed Tomography of LAPC4-CR Castration-Resistant Prostate Cancer Xenograft Model in Soft Tissue Compartments[1]

Keisha C. McCall[*,†], Su-Chun Cheng[‡], Ying Huang[§], Nancy E. Kohl[†,2], Tanya Tupper[†], Annick D. Van den Abbeele[*,†,¶], Katherine A. Zukotynski[#] and Christopher J. Sweeney[§,]**

*Department of Imaging, Dana-Farber Cancer Institute, 450 Brookline Ave, Boston, MA, 02215, USA; †Center for Biomedical Imaging in Oncology (Lurie Family Imaging Center), Dana-Farber Cancer Institute, 450 Brookline Ave, Boston, MA, 02215, USA; ‡Department of Biostatistics & Computational Biology, Dana-Farber Cancer Institute, 450 Brookline Ave, Boston, MA, 02215, USA; §Department of Medical Oncology, Dana-Farber Cancer Institute, 450 Brookline Ave, Boston, MA, 02215, USA; ¶Department of Radiology, Brigham and Women's Hospital, Harvard Medical School, 75 Francis St, Boston MA 02115, USA; #Department of Medical Imaging, Sunnybrook Hospital, University of Toronto, 263 McCaul St–4th Floor, Toronto, Ontario M5T 1W7, Canada; **Department of Medicine, Brigham and Women's Hospital, Harvard Medical School, 75 Francis St, Boston MA 02115, USA

Abstract

Preclinical xenograft models have contributed to advancing our understanding of the molecular basis of prostate cancer and to the development of targeted therapy. However, traditional preclinical *in vivo* techniques using caliper measurements and survival analysis evaluate the macroscopic tumor behavior, whereas tissue sampling disrupts the microenvironment and cannot be used for longitudinal studies in the same animal. Herein, we present an *in vivo* study of [18F]-fluorodeoxyglucose (FDG) positron emission tomography (PET)/computed tomography (CT) designed to evaluate the metabolism within the microenvironment of LAPC4-CR, a unique murine model of castration-resistant prostate cancer. Mice bearing LAPC4-CR subcutaneous tumors were administered [18F]-FDG via intravenous injection. After a 60-minute distribution phase, the mice were imaged on a PET/CT scanner with submillimeter resolution; and the fused PET/CT images were analyzed to evaluate tumor size, location, and metabolism across the cohort of mice. The xenograft tumors showed [18F]-FDG uptake that was independent of tumor size and was significantly greater than uptake in skeletal muscle and liver in mice (Wilcoxon signed-rank *P* values of .0002 and .0002, respectively). [18F]-FDG metabolism of the LAPC4-CR tumors was 2.1 ± 0.8 ID/cm^3*wt, with tumor to muscle ratio of 7.4 ± 4.7 and tumor to liver background ratio of 6.7 ± 2.3. Noninvasive molecular imaging techniques such as PET/CT can be used to probe the microenvironment of tumors *in vivo*. This study showed that [18F]-FDG-PET/CT could be used to image and assess glucose metabolism of LAPC4-CR xenografts *in vivo*. Further work can investigate the use of PET/CT to quantify the metabolic response of LAPC4-CR to novel agents and combination therapies using soft tissue and possibly bone compartment xenograft models.

Translational Oncology (2015) 8, 147–153

Address all correspondence to: Keisha C. McCall, PhD, Department of Imaging, Dana-Farber Cancer Institute, 450 Brookline Ave, Boston, MA, 02215, USA. E-mail: kmccall@partners.org

[1] Funding: Dana-Farber/Harvard Cancer Center SPORE (Specialized Program of Research Excellence) in Prostate Cancer, Developmental Project, NIH5P50 CA090381-10.

[2] Dr Kohl has currently moved to Blueprint Medicines, 215 First St, Cambridge, MA 02142, USA, as the Vice President of Biology.

Received 6 February 2015; Revised 26 March 2015; Accepted 30 March 2015

1936-5233/15
http://dx.doi.org/10.1016/j.tranon.2015.03.004

Introduction

Prostate cancer is the second leading cause of cancer death in American men [1]. Nearly all prostate cancer deaths are due to metastatic disease that has emerged once the disease becomes resistant to castration and is referred to as *castration-resistant prostate cancer* (CRPC). The drivers of prostate cancer cell proliferation, metastasis, and evasion of apoptosis include activation of the androgen receptor, carcinogenic signaling within cells, and the effect of survival signals from the microenvironment. Regression or stabilization of cancer burden occurs in some CRPC patients through the use of hormonal therapy [2,3], cytotoxic therapy [4,5], and immune-based therapy [6] that abrogates one or more of these drivers. An alpha-emitting radiopharmaceutical [7] is also currently used clinically in CRPC patients with skeletal metastases to prolong overall survival and localized radiation cell killing in bone metastases. Metastatic CRPC will typically progress despite therapy as a result of redundant or adaptive resistance mechanisms. Improvements in patient outcomes will require preventing resistance through multitargeted approaches against the key drivers of prostate cancer. As such, there is a need for informative *in vivo* studies of CRPC.

Preclinical xenograft models of CRPC have contributed toward advancing the understanding of the molecular basis of the disease, as well as developing and testing innovative therapies. However, traditional preclinical investigative methods of tumor volume measurements and survival studies provide no information about the molecular basis of tumor response to therapy or development of resistance, whereas tissue sampling and histochemical assays have limited use for longitudinal studies. Noninvasive *in vivo* molecular imaging techniques such as positron emission tomography (PET)/computed tomography (CT) can be used to probe the microenvironment in preclinical models of cancer and in clinical cancer patients.

[18F]-fluorodeoxyglucose (FDG) is taken up by tumor cells according to the glycolytic rate (Warburg effect). Therefore, [18F]-FDG-PET/CT may be used to assess the extent of malignancy and detect disease in both soft tissue and osseous compartments, and could serve as a biomarker for assessment of treatment response and outcome measures in CRPC. [18F]-FDG-PET was able to assess treatment effects that would usually only be appreciated by a combination of prostate-specific antigen, [99mTc]-methylene diphosphonate bone scan, and anatomic imaging in patients being treated for CRPC [8]. The intensity of [18F]-FDG and [99mTc]-methylene diphosphonate uptake at osseous sites of disease, on PET and bone scan, respectively, was found to be prognostic of overall survival in patients with metastatic prostate cancer [9]. [18F]-FDG uptake measured at baseline in bone and soft tissue metastases on PET was also reported to be prognostic of overall survival in patients with CRPC [10]. Serial [18F]-FDG-PET/CT also allows longitudinal assessment within a single subject or group of subjects within a cohort, with highly reproducible measurement [11–14].

This article presents the results of an investigation of [18F]-FDG-PET/CT as a noninvasive imaging method of LAPC4-CR, the preclinical model of the aggressive CRPC subtype. In published preclinical studies of hormone-independent (PC-3, DU145) and -dependent (CWR22, PAC120) cell lines, [18F]-FDG-PET was found to be an effective *in vivo* imaging method for assessing response to androgen deprivation for PC-3 and CWR22 xenografts [15]. [18F]-FDG-PET has also been investigated for imaging the androgen-dependent wild-type LAPC4 cell line in xenograft models [16]. However, to our knowledge, this is the first publication of *in vivo* [18F]-FDG-PET/CT imaging of the castrate-resistant LAPC4-CR xenograft model.

Methods and Materials

All experiments were performed in accordance to institutional animal care and use committee guidelines established at the Dana-Farber Cancer Institute and conducted within the barrier facility at the Lurie Family Imaging Center of the Center for Biomedical Imaging in Oncology (CBIO/LFIC).

In February 2013, 6-week-old female Nu/Nu mice were housed in cages equipped with filtered ventilation and watering systems, with free access to food and environmental enrichment, and kept in climate-controlled negative pressure rooms with 12-hour circadian light/dark cycles. LAPC4-CR tumor fragments of size of approximately 2 mm^3 (approximately 1 million cells) were surgically implanted subcutaneously in the right flank of 20 mice. Growth of the implanted tumors was monitored biweekly, and tumor volumes were estimated from caliper measurements as $\frac{1}{2}*L*W^2$. Mice were imaged when tumor volume reached a size of approximately 100 mm^3, which occurred between 5 and 14 weeks after the implantation of tumor fragments for 13 of the 20 mice. All 20 implanted mice developed subcutaneous tumors; however, the tumor size in 7 mice remained too small to meet the imaging protocol criteria. Mice were humanely sacrificed using institutional animal care and use committee–approved methods after imaging.

The 13 mice bearing LAPC4-CR subcutaneous tumors larger than 100 mm^3 were imaged with [18F]-FDG-PET/CT. The mice were intravenously administered 331 ± 50 μCi (12.2 ± 1.85 MBq) of [18F]-FDG via a lateral tail vein injection as an approximately 100-μL bolus followed by a 100- to 200-μL flush with phosphate-buffered saline. [18F]-FDG was manufactured by a commercial radiopharmaceutical manufacturer (PETNET Solutions Inc) and supplied in ethanol-stabilized sodium chloride solution. Mice were imaged 61 ± 1 minutes after the injection to produce images with good tumor contrast by allowing time for accumulation of [18F]-FDG within metabolically active tissue and clearance from surrounding muscle and blood pool. This uptake period (time between radiotracer injection and image acquisition initiation) was kept consistent for all mice to ensure that the radiotracer distribution was at similar point of the plateau in [18F]-FDG pharmacokinetics, where tumor uptake was slowly rising and background tissue uptake was slowly decreasing.

Mouse preparation protocol factors such as anesthesia, external warming, and restricted diets or fasting affect intersubject variation in [18F]-FDG metabolism and biodistribution in mice [17]. Therefore, the mice were placed in clean cages and fed a high-fat, low-protein, and low-carbohydrate ketogenic diet with free access to water for 12 to 16 hours before the [18F]-FDG-PET/CT. The mice were anesthetized using an inhaled anesthesia (2%-3% sevoflurane and air) during the injection of radiotracer and were kept unconscious during the uptake period and imaging to minimize intersubject variation in [18F]-FDG metabolism in skeletal muscle and cerebrum. Warming was used to maintain healthy core body temperature of the nude mice during periods of unconsciousness and to minimize brown-fat metabolism from hypothermia. Therefore, the mice were warmed for 1 hour on circulating warm water heating pads before bring injected with radiotracer and were kept warm throughout the unconscious uptake phase and during image acquisition.

All images were acquired using an Inveon Multi-Modality scanner (Siemens Medical Solutions USA, Inc), a small-animal PET/CT system that has a lutetium oxyorthosilicate detector PET camera with 36 cps/kBq sensitivity and nominal spatial resolution of 1.6 mm full width at half maximum [18], and a cone-beam CT camera capable of high-resolution CT imaging up to 15-μm resolution. For *in vivo*

PET/CT, a low radiation–dose CT protocol was used to acquire 0.2-mm pixel size CT images for anatomic localization and tumor volume measurement. CT projections were acquired in step and shoot beams at 1° intervals over a 210° arc, using 80-kVp 0.5-mA cone-beam x-rays and 0.135 seconds per projection. The PET images were acquired as 10-minute static acquisitions using detector settings of 350 to 650 keV energy window, a 3.432-nanosecond coincidence timing window, and the full 38° axial acceptance angle to increase the number of acquired positron emission counts and reduce image noise. CT images were reconstructed using a Feldkamp convolution-back-projection algorithm, whereas PET images were reconstructed with a combined iterative algorithm of three-dimensional Ordered Subset Expectation Maximization and maximum *a posteriori* estimation for uniform spatial resolution recovery to 0.8 mm full width at half maximum. Image fusion and analysis were done on an Inveon Research Workstation (Siemens Medical Solutions USA, Inc) and Hermes Hybrid Viewer (HERMES Medical Solutions).

PET image values were normalized by the administered radioactivity of the tracer adjusted for physical decay (injected dose) and the body weight of the mouse. The body weight of each mouse was measured and recorded on the day of imaging, and used as an estimate of the volume of distribution or total volume of tissue into which the radiotracer was distributed during the uptake period. The normalized PET value is sometimes referred to as the *standardized uptake value*, a semiquantitative measurement of [^{18}F]-FDG metabolism in clinical imaging, or the ID/cm^3*wt in preclinical imaging, and is calculated according to Eq. (1):

$$\text{I.D./cm}^3\text{*wt}\left[{}^{\text{g}}/_{\text{cm}^3}\right] = \left(\text{PET image value}\left[\frac{\text{MBq}}{\text{cm}^3}\right] \Big/ \text{injected dose [MBq]}\right) \times \text{body weight [g]}$$

The [^{18}F]-FDG-PET/CT images were evaluated to determine anatomic and metabolic tumor volumes and the metabolism in tumor versus the background metabolism in normal tissue. Fused PET/CT images were used to locate the tumor, organs, and other tissues. The CT images were used to delineate the anatomic boundary for the volumes of interest (VOIs), whereas the PET images were used to measure the [^{18}F]-FDG metabolism (ID/cm^3*wt) in the VOIs. The anatomic tumor volume was defined from the CT images by drawing a 3D ellipsoid VOI to just enclose the subcutaneous lesion, as shown in Figure 1(*A*). The metabolic tumor volume of the lesion was defined as the VOI where the [^{18}F]-FDG metabolism was at least 70% of the maximum value measured within that lesion. The metabolic tumor volume thus excluded necrotic regions of the tumor, scar tissue, calcification, and other metabolically inactive tissues, as shown in Figure 1(*B*). The [^{18}F]-FDG metabolism was reported as a maximum (max) and mean (mean70%) ID/cm^3*wt within the metabolic tumor volume. The background [^{18}F]-FDG metabolism in normal muscle and in normal liver parenchyma was measured by placing a 3-mm-diameter sphere VOI within the flank muscle contralateral to the xenograft and within the right hepatic lobe 2 to 3 mm inferior from the diaphragm. The mean within the liver VOI was used to calculate the tumor to background ratio, TBR [ID/cm^3*wt]/liver, and the mean in skeletal muscle VOI was used to calculate the tumor to muscle ratio, TMR [ID/cm^3*wt]/muscle, of Table 1. During image analysis, each tumor was segmented into 30 spatial subregions, and the local maximum [^{18}F]-FDG uptake was measured within each subregion. The intratumor heterogeneity of metabolism was then calculated as the range, interquartile range (IQR), and the percentage differences between the quartiles of local maximum [^{18}F]-FDG uptake in the subregions, as shown in Table 1.

Results

The mice showed the expected biodistribution of [^{18}F]-FDG in normal tissues, with radiotracer uptake seen in cardiac muscle, cerebellum, and harderian glands as well as physiologic excretion via the kidneys and urinary bladder (Figure 2). There was homogeneous [^{18}F]-FDG activity in the liver and skeletal muscle. There was moderate to high [^{18}F]-FDG activity in the LAPC4-CR xenografts compared with adjacent soft tissue liver and muscle (Figure 3 and Table 1). The xenograft metabolism was 4 to 11 times higher than liver, 3 to 19 times higher than muscle (Table 1), and significantly higher than normal tissue (Wilcoxon signed-rank P value < .01, Figure 4). The intratumor heterogeneity, IQR of local metabolism in subregions within the xenografts, was 78 ± 39% (Table 1). The [^{18}F]-FDG-PET/CT images of 12 tumors showed enhanced [^{18}F]-FDG activity at the rim and a photopenic center suspicious of necrosis. The tumor with the smallest CT tumor volume, mouse ID# 04F01 with 81 mm^3, did not show the imaging characteristics of a necrotic core; however, the [^{18}F]-FDG metabolism in that tumor fell within the range of the other tumors (Figure 5*A* and Table 1).

The [^{18}F]-FDG activity in the LAPC4-CR xenograft was not dependent on tumor size, and there was no correlation of [^{18}F]-FDG metabolism and anatomic or metabolic tumor volume (Figure 5). [^{18}F]-FDG metabolism was also not dependent on the number of days any of the tumors required to grow to greater than 100 mm^3 in size (Figure 5). The anatomic tumor volume measured by CT was 188 ± 62 mm^3. The tumor volumes estimated using calipers and the tumor volumes measured on CT images were similar (Wilcoxon signed-rank P value = .06), but there was no significant concordance between the values (Spearman ρ = 0.4, P value = .1). The metabolically active tumor was smaller than the anatomic tumor volume (Figure 1*B*). The metabolic volume of the LAPC4-CR xenograft was 16.5 ± 11.8 mm^3 with [^{18}F]-FDG metabolism (mean 70%) 2.1 ± 0.8 [ID/cm^3*wt] (Table 1).

Discussion

The data detailed above provide the experimental details used to enable the evaluation of a new prostate cancer cell line xenograft by [^{18}F]-FDG-PET/CT. Our preclinical [^{18}F]-FDG-PET/CT protocol included several animal handling considerations that are necessary to improve image quality and lesion detectability and to maintain consistent physiologic [^{18}F]-FDG uptake in mice. High blood glucose concentrations are associated with hyperinsulinemia and resulting altered biodistribution with preferential [^{18}F]-FDG uptake in skeletal muscles [19]. Basal blood glucose level can be reduced in preclinical and clinical studies through many hours of fasting; however, a ketogenic diet of high fat, low protein, and low carbohydrate was used as an alternative to fasting in tumor-bearing mice. In a conference abstract from researchers at the CBIO/LFIC, the ketogenic diet resulted in similar low basal blood glucose level within cohorts of mice, whereas hypoglycemia was observed in some fasted mice [20]. Because hyperthermia increases the incidence of metabolically active brown adipose tissue in rodents [17,21,22], the body temperature of the mice was controlled with external heating. Likewise, injected ketamine anesthesia is associated with increased metabolically active brown adipose tissue in rodents and elevated

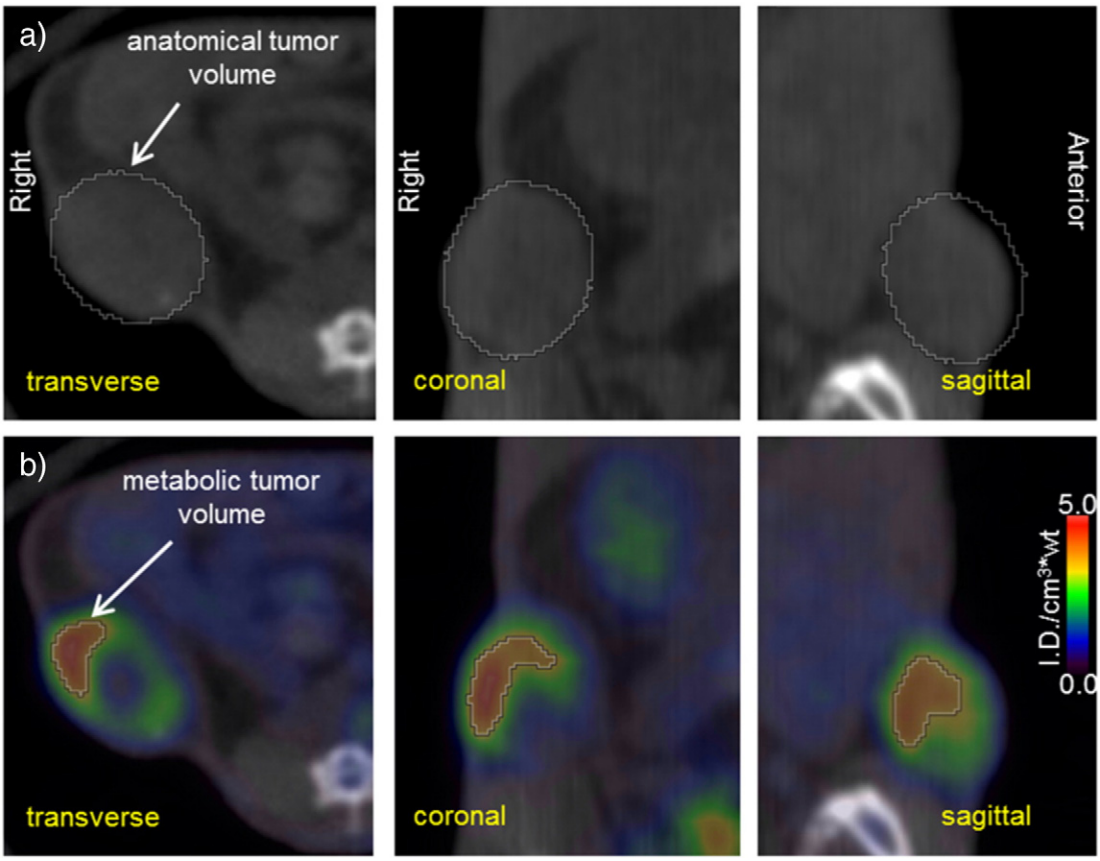

Figure 1. Orthogonal CT (a) and fused [18F]-FDG-PET/CT (b) views of a subcutaneous LAPC4-CR tumor in a murine xenograft model. The anatomic tumor volume was estimated by drawing a 3D ellipsoid around the visible tumor boundary on the CT images. The metabolic tumor volume was estimated by determining the volume of the anatomic tumor that had [18F]-FDG uptake of at least 70% of the maximum uptake within the tumor (70% threshold).

Table 1. Results of the Analysis of Tumor Volume and Tumor Metabolism in LAPC4-CR Xenograft Models Using [18F]-FDG-PET/CT

Mouse ID	Tumor Growth	Caliper Volume Estimate	CT Tumor Volume	FDG Metabolic Volume	FDG Metabolism Max	FDG Metabolism Mean70%	TBR Mean70%/ Liver	TMR Mean70%/ Muscle	Intratumor Heterogeneity		
	(d)	(mm^3)	(mm^3)	(mm^3)	(ID/cm^3 wt)	(ID/cm^3 wt)	(ID/cm^3 wt)/liver	(ID/cm^3 wt)/muscle	Range (ID/cm^3 wt)	IQR (ID/cm^3 wt)	IQR (%)
03A00	35	133.1	206.0	19.4	4.39	3.50	10.3	19.5	4.2	1.9	121%
03A01	35	111.6	160.2	30.9	1.84	1.49	4.7	4.0	1.5	0.5	42%
03B00	43	156.8	228.2	5.0	2.73	2.18	7.5	4.4	1.9	0.6	50%
03B01	43	185.7	247.1	12.8	1.93	1.51	3.6	3.6	1.3	0.5	58%
03C00	43	116.6	167.7	6.2	2.95	2.38	6.6	10.8	2.6	1.0	119%
03C01	43	113.1	222.7	23.4	1.82	1.42	5.1	5.5	1.4	0.5	52%
03C03	43	152.6	122.0	4.3	1.75	1.37	4.6	8.1	1.3	0.5	83%
04F01	49	158.1	81.3	6.8	3.68	2.97	8.5	7.2	3.2	1.7	179%
04F03	49	210.7	253.2	37.5	2.37	1.90	6.3	3.0	2.0	0.8	59%
04A00	84	93.8	100.8	2.3	1.59	1.29	4.2	5.0	1.4	0.4	65%
04C00	84	161.4	278.7	27.1	3.82	2.99	10.7	9.0	3.3	1.0	51%
04E03	84	168.8	148.2	11.0	2.16	1.73	6.7	3.3	1.4	0.7	72%
04F00	98	NA	227.5	27.8	3.96	3.05	8.5	12.7	3.2	1.2	59%
Mean ± standard deviation		146.9 ± 34.2	188.0 ± 62.4	16.5 ± 11.8	2.7 ± 1.0	2.1 ± 0.8	6.7 ± 2.3	7.4 ± 4.7	2.2 ± 1.0	0.9 ± 0.5	78% ± 39%
Median		154.7	206.0	12.8	2.4	1.9	6.6	5.5	1.9	0.7	59%
95% CI of median		[113.1, 168.8]	[122.0, 247.1]	[5.0, 27.8]	[1.8, 3.8]	[1.4, 3.0]	[4.6, 8.5]	[3.6, 10.8]	[1.4, 3.2]	[0.5, 1.2]	[51%, 119%]

The [18F]-FDG metabolism in tumors was measured as the maximum (max) and mean (mean70%) [18F]-FDG uptake within the anatomic tumor volume. Across the cohort, [18F]-FDG uptake was normalized by the injected activity and body weight of the individual mouse (ID/cm^3*wt). Tumor metabolism was compared to background metabolism in healthy liver, expressed as the TBR (ID/cm^3*wt)/liver, and compared to skeletal muscle in a contralateral limb, expressed as the TMR (ID/cm^3*wt)/muscle. The intratumor heterogeneity was calculated by comparing local maxima [18F]-FDG metabolism of subregions within each tumor and was expressed as the differences between highest and lowest of the subregions (range) and between the quartiles (IQR).

NA indicates that caliper measurements were not recorded at the time of imaging.

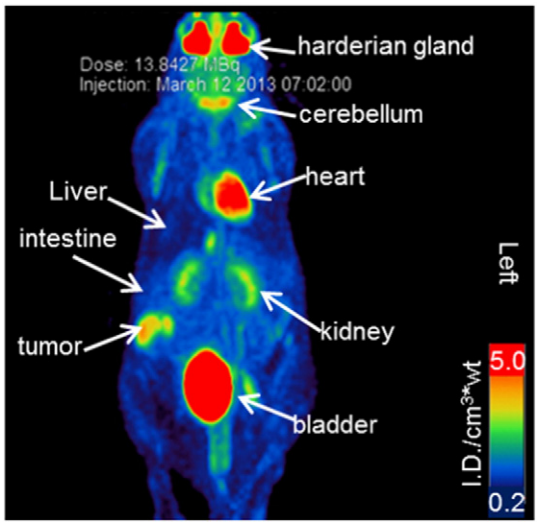

Figure 2. [^{18}F]-FDG biodistribution in mice with LAPC4-CR tumors. Maximum intensity projection of the [^{18}F]-FDG PET image acquired at 60 minutes after injection of the radiotracer. The [^{18}F]-FDG uptake has been normalized by the injected activity and the mouse body weight ([ID/cm^3*wt]) and is shown using a false-color linear scale for visual contrast. There is an expected biodistribution of radiotracer with activity in normal tissue and physiologic radiotracer excretion. Radiotracer uptake was also noted in the subcutaneous tumor.

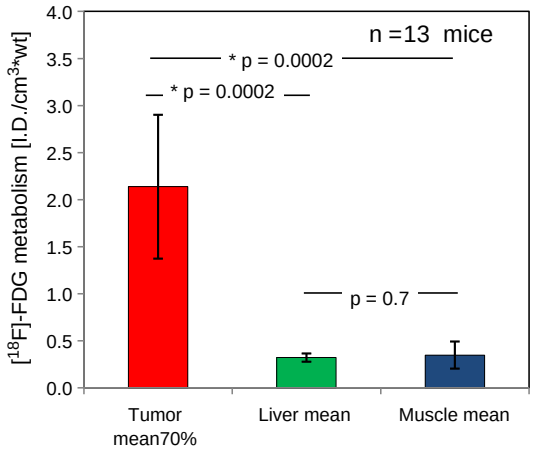

Figure 4. [^{18}F]-FDG metabolism measurements in LAPC4-CR xenograft tumors and in normal background tissues. Bar plots indicate the mean uptake across the cohort of 13 mice. The standard deviation between mice is indicated by the error bars. *Significant *P* values ($P < .01$) in Wilcoxon signed-rank analysis.

blood glucose levels [17,22]; therefore, the mice were anesthetized using an inhaled anesthesia (2%-3% sevoflurane and air) for [^{18}F]-FDG-PET/CT studies.

Of note, the small size of the mouse muscles renders the analysis of radiotracer uptake prone to partial volume averaging errors because small regions of fat, skin, or pelvic organs may be included within the region of interest (ROI). Additionally, excreted [^{18}F]-FDG and metabolites in the urinary bladder introduce uncertainty due to "spill-in" included in the ROI. The most uniform tissue ROI across our cohort of mice was found to be the liver because the size of the liver allowed consistent measurements with minimal partial volume averaging effects.

A shared reference location defined the coordinates in image space for the PET and CT; this allowed automatic and precise image registration and PET/CT image fusion for image analysis. However, in each mouse, the accuracy of image registration was verified by

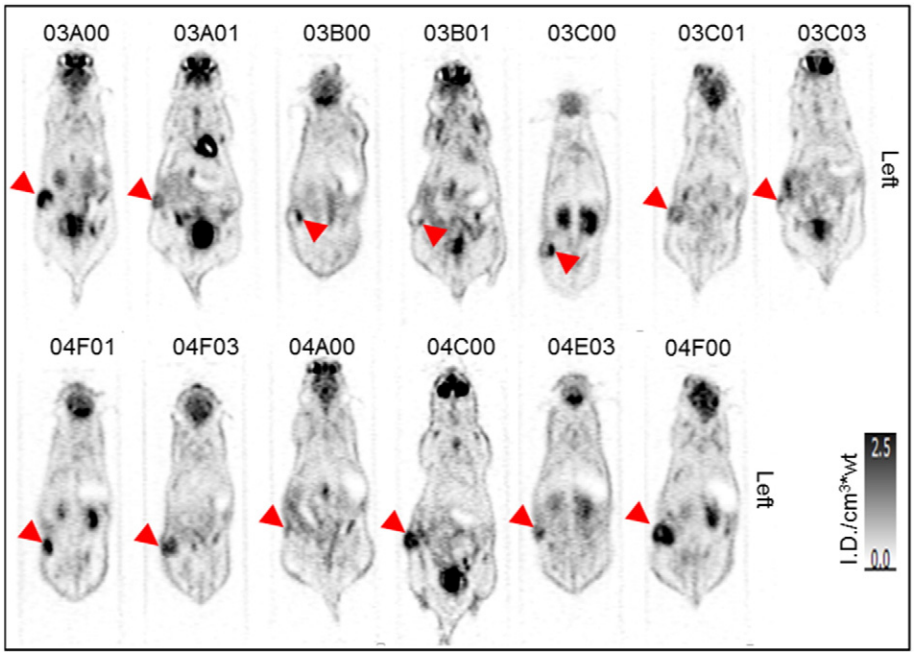

Figure 3. [^{18}F]-FDG metabolism in LAPC4-CR xenograft tumors in 13 mice. Figures show a coronal slice through the region of highest [^{18}F]-FDG uptake within each subcutaneous tumor, as indicated by arrowheads. [^{18}F]-FDG PET images were acquired at 60 minutes after injection of the radiotracer and displayed on a linear gray scale normalized by the injected activity and the mouse body weight ([ID/cm^3*wt]).

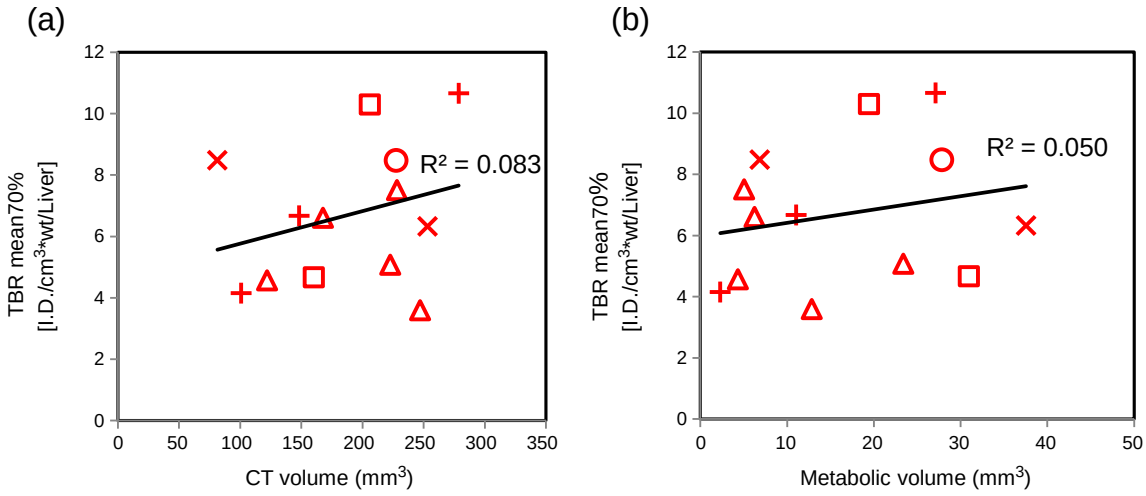

Figure 5. [18F]-FDG metabolism in LAPC4-CR xenograft tumors compared to anatomic and metabolic tumor volume measured on PET/CT. Scatter plots show (a) [18F]-FDG metabolism versus anatomic tumor volume seen on CT and (b) [18F]-FDG metabolism versus metabolic tumor volume seen on PET. The symbols represent the day postimplantation of tumors: 35 days (squares), 43 days (triangles), 49 days (Xs), 84 days (crosses), and 98 days (circles). The best-fit linear correlations for the pooled data of the 13 xenograft tumors are also shown.

visual inspection using several images in orthogonal views to ensure that no motion during imaging or errors during reconstruction or fusion had occurred. The fused PET/CT and CT images provided a more accurate estimate of 3D tumor volumes than can be calculated from physical palpation and caliper measurements. In addition, the fused PET/CT images allowed better evaluation of regions of active tumor metabolism. Fused PET/CT images showed regions within the tumor mass where there was little or no [18F]-FDG uptake, often located near the center of the subcutaneous mass, which was a characteristic of soft tissue/tumor necrosis. Other metabolically inactive regions coincided with small localized regions of calcified tissue on the CT images. The presence of necrotic cores and calcification of dead tissue in the LAPC4-CR cell line xenograft tumors was found in earlier histopathology studies, which were done on another cohort of mice during the development of the cell line. Examples of stained tumor sections from that prior study, which illustrates the typical pathology of LAPC4-CR xenografts, are shown in Figure 6.

Conclusion

This study reports the results of [18F]-FDG-PET/CT in a xenograft model of the castration-resistant prostate tumor line LAPC4-CR. The xenograft tumors showed [18F]-FDG uptake that was significantly greater than uptake of skeletal muscle and liver. In addition, the intensity of [18F]-FDG uptake was independent of anatomic tumor size and metabolic tumor volume. Further work will investigate the use of [18F]-FDG-PET/CT to quantify the response of LAPC4-CR to novel agents and combination therapies using soft tissue and possibly bone compartment xenograft models.

Acknowledgements

This work was supported by the Dana-Farber/Harvard Cancer Center SPORE (Specialized Program of Research Excellence) in Prostate Cancer, Developmental Project, NIH5P50 CA090381-10. The authors also acknowledge the following individuals for their contributions: Michaela Bowden, PhD, at Dana-Farber Cancer Institute, coordinated laboratory experiments and facilitated access to

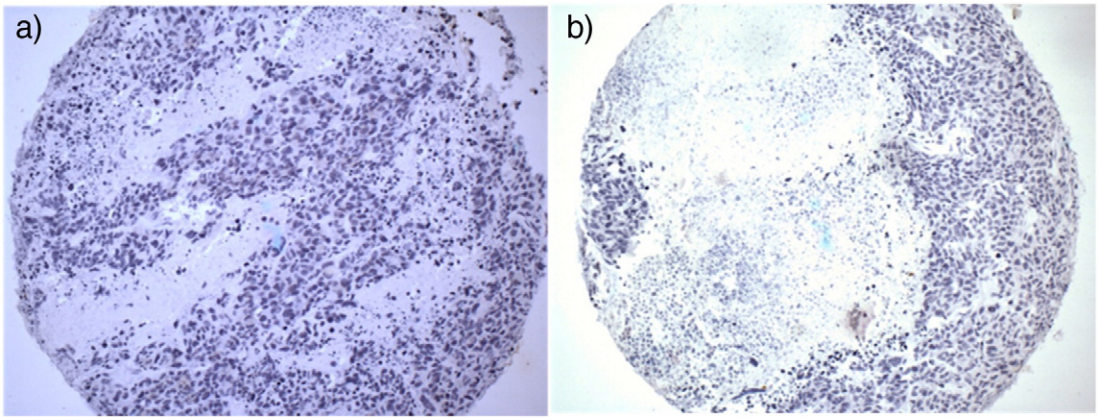

Figure 6. Hematoxylin-stained tissue sections of LAPC4-CR xenografts with the nuclei of tumor cells stained deep purple. Amorphous areas with a lack of staining indicate the acellular regions of necrosis. Slide (a) shows small regions of necrosis within the tumor tissue, whereas (b) shows a tumor that had developed a necrotic core.

histological images on LAPC4-CR tumor models; Su-Chun Cheng, PhD, Biostatistician at the Department of Biostatistics, Dana-Farber Cancer Institute, provided expert advice on statistical analysis methods; Amanda Christie, Research Technician at the CBIO/LFIC, provided advice on small-animal handling and on tumor growth patterns for Nu/Nu murine LAPC4-CR models, and prepared tumor fragments for implantation; Ying Huang, MD, PhD, Scientist at Dana-Farber Cancer Institute, performed hematoxylin staining and analysis and provided representative histological images of LAPC4-CR xenograft tumors; Li Jia, PhD, Scientist at Dana-Farber Cancer Institute, provided expertise in the LAPC4-CR cell line and prostate cancer tumor models; Paul T. Kirschmeier, PhD of the Belfer Institute for Applied Cancer Science, Dana-Farber Cancer Institute, and the CBIO/LFIC provided scientific advice and facilitated access to experimental data and images; Quang-De Nguyen, PhD, Director at the CBIO/LFIC, provided expert scientific advice and facilitated access to experimental data and images; Lei Qin, PhD, MRI Physicist at Department of Imaging, Dana-Farber Cancer Institute, provided imaging expertise in image acquisition and interpretation; Tanya Tupper, Research Technician at the CBIO/LFIC, conducted the preclinical data acquisition for this experiment, including small-animal handling, and subcutaneous tumor implantation, tumor growth monitoring, animal health monitoring, and *in vivo* PET/CT imaging of the mice; Jeffery Yap, PhD, contributed to the experiment design and defined the preclinical PET/CT imaging protocols as the Senior Diagnostic Physicist at the Department of Imaging, Dana-Farber Cancer Institute, and the CBIO/LFIC. Dr Yap is currently Associate Director of the Center for Quantitative Cancer Imaging at the Huntsman Cancer Center Institute, University of Utah.

References

[1] Siegel R, Naishadham D, and Jemal A (2013). Cancer statistics, 2013. *CA Cancer J Clin* **63**, 11–30.

[2] de Bono JS, Logothetis CJ, Molina A, Fizazi K, North S, Chu L, Chi KN, Jones RJ, Goodman Jr OB, and Saad F, et al (2011). Abiraterone and increased survival in metastatic prostate cancer. *N Engl J Med* **364**, 1995–2005.

[3] Scher H, Fizazi K, Saad S, Taplin M, Sternberg CN, Miller K, De Wit R, Mulders P, Hirmand M, and Selby B, et al (2012.). MDV3100, an androgen receptor signaling inhibitor (ARSI), improves overall survival in patients with prostate cancer post docetaxel; results from the Phase 3 AFFIRM Study. GU ASCO; 2012.

[4] Tannock IF, de Wit R, Berry WR, Horti J, Pluzanska A, Chi KN, Oudard S, Theodore C, James ND, and Turesson I, et al (2004). Docetaxel plus prednisone or mitoxantrone plus prednisone for advanced prostate cancer. *N Engl J Med* **351**, 1502–1512.

[5] de Bono JS, Oudard S, Ozguroglu M, Hansen S, Machiels JP, Kocak I, Gravis G, Bodrogi I, Mackenzie MJ, and Shen L, et al (2010). Prednisone plus cabazitaxel or mitoxantrone for metastatic castration-resistant prostate cancer progressing after docetaxel treatment: a randomised open-label trial. *Lancet* **376**, 1147–1154.

[6] Kantoff PW, Higano CS, Shore ND, Berger ER, Small EJ, Penson DF, Redfern CH, Ferrari AC, Dreicer R, and Sims RB, et al (2010). Sipuleucel-T immunotherapy for castration-resistant prostate cancer. *N Engl J Med* **363**, 411–422.

[7] Parker C, Heinrich D, O'Sullivan JM, Fosså S, Chodacki A, Demkow T, Cross A, Bolstad B, Garcia-Vargas J, and Sartor O (2011). Overall survival benefit of radium-223 chloride (Alpharadin) in the treatment of patients with symptomatic bone metastases in castration-resistant prostate cancer (CRPC): a phase III randomised trial (ALSYMPCA). Proceedings of ECCO/ESMO Annual Meeting; 2011.

[8] Morris MJ, Akhurst T, Larson SM, Ditullio M, Chu E, Siedlecki K, Verbel D, Heller G, Kelly WK, and Slovin S, et al (2005). Fluorodeoxyglucose positron emission tomography as an outcome measure for castrate metastatic prostate cancer treated with antimicrotubule chemotherapy. *Clin Cancer Res* **11**, 3210–3216.

[9] Meirelles GSP, Schöder H, Ravizzini GC, Gönen M, Fox JJ, Humm J, Morris MJ, Scher HI, and Larson SM (2010). Prognostic value of baseline [18F] fluorodeoxyglucose positron emission tomography and 99mTc-MDP bone scan in progressing metastatic prostate cancer. *Clin Cancer Res* **16**, 6093–6099.

[10] Jadvar H, Desai B, Ji L, Conti PS, Dorff TB, Groshen SG, Pinski JK, and Quinn DI (2013). Baseline 18F-FDG PET/CT parameters as imaging biomarkers of overall survival in castrate-resistant metastatic prostate cancer. *J Nucl Med* **54**, 1195–1201.

[11] Nahmias C and Wahl LM (2008). Reproducibility of standardized uptake value measurements determined by 18F-FDG PET in malignant tumors. *J Nucl Med* **49**, 1804–1808.

[12] Weber WA, Ziegler SI, Thodtmann R, Hanauske A-R, and Schwaiger M (1999). Reproducibility of metabolic measurements in malignant tumors using FDG PET. *J Nucl Med* **40**, 1771–1777.

[13] Dandekar M, Tseng JR, and Gambhir SS (2007). Reproducibility of 18F-FDG microPET studies in mouse tumor xenografts. *J Nucl Med* **48**, 602–607.

[14] Whisenant JG, Peterson TE, Fluckiger JU, Tantawy MN, Ayers GD, and Yankeelov TE (2013). Reproducibility of static and dynamic 18F-FDG, 18F-FLT, and 18F-FMISO microPET studies in a murine model of HER2+ breast cancer. *Mol Imaging Biol* **15**, 87–96.

[15] Kukuk D, Reischl G, Raguin O, Wiehr S, Judenhofer MS, Calaminus C, Honndorf VS, Quintanilla-Martinez L, Schönberger T, and Duchamp O, et al (2011). Assessment of PET tracer uptake in hormone-independent and hormone-dependent xenograft prostate cancer mouse models. *J Nucl Med* **52**, 1654–1663.

[16] Emonds KM, Swinnen JV, Lerut E, Koole M, Mortelmans L, and Mottaghy FM (2013). Evaluation of androgen-induced effects on the uptake of [18F] FDG,[11C] choline and [11C] acetate in an androgen-sensitive and androgen-independent prostate cancer xenograft model. *EJNMMI Res* **3**, 31.

[17] Fueger BJ, Czernin J, Hildebrandt I, Tran C, Halpern BS, Stout D, Phelps ME, and Weber WA (2006). Impact of animal handling on the results of 18F-FDG PET studies in mice. *J Nucl Med* **47**, 999–1006.

[18] Brad JK, Carrie BH, Aaron RM, Mark WL, and Val JL (2009). NEMA NU 2-2007 performance measurements of the Siemens Inveon™ preclinical small animal PET system. *Phys Med Biol* **54**, 2359.

[19] Lindholm P, Minn H, Leskinen-Kallio S, Bergman J, Ruotsalainen U, and Joensuu H (1993). Influence of the blood glucose concentration on FDG uptake in cancer—a PET study. *J Nucl Med* **34**, 1–6.

[20] Tupper T, Yap JT, Franchetti Y, McDonagh E, Locascio TA, Kung A, and Wang Y (2011). Utilizing ketogenic diet as an alternative to fasting in preclinical 18F-FDG PET. World Molecular Imaging Congress (San Diego, 2011); 2011.

[21] Weber WA (2004). Brown adipose tissue and nuclear medicine imaging. *J Nucl Med* **45**, 1101–1103.

[22] Tatsumi M, Engles JM, Ishimori T, Nicely OB, Cohade C, and Wahl RL (2004). Intense 18F-FDG uptake in brown fat can be reduced pharmacologically. *J Nucl Med* **45**, 1189–1193.